REPORT 1208

A COMPARISON OF THE SPANWISE LOADING CALCULATED BY VARIOUS METHODS WITH EXPERIMENTAL LOADINGS OBTAINED ON A 45° SWEPTBACK WING OF ASPECT RATIO 8.02 AT A REYNOLDS NUMBER OF 4.0×10^6 †

By William C. Schneider

SUMMARY

Experimental force and moment data obtained by pressure measurements on a wing of aspect ratio 8.02, 45° sweepback of the quarter-chord line, taper ratio of 0.45, and NACA 63_1A012 airfoil sections have been compared with the calculated loadings obtained by the standard methods proposed by Weissinger, Falkner, and Multhopp, as well as by several variations of these methods. The most accurate shape of the span load distribution was predicted by the standard Multhopp 23×1 solution. The standard Falkner 6×3 solution failed to predict the experimental dip in the span load distribution at the root stations. All methods that predicted a fairly accurate loading shape predicted the lift-curve slope about 8 percent low. Since all the methods are based on thin-wing theory, the underestimation of the lift-curve slope is probably attributable to the finite thickness of the wing. On the basis of the present calculations, the Weissigner method, when the number of control points was increased from 7 (the number suggested by Weissinger) to 15, or the Multhopp method, when using at least 15 control points, is a good compromise between accuracy of the results and time required for a solution.

INTRODUCTION

Various methods exist for the calculation of aerodynamic forces on swept wings but only limited experimental corroboration of the different approaches has been made. As early as 1947, a comparison with experiment was made of the various methods available at that time (ref. 1), but the comparison was limited to experimental data obtained on wings of low aspect ratio; and, in addition, the experimental load shape was somewhat inadequately defined by the small number of spanwise stations available. No comparisons have previously been made for wings having both high aspect ratio and large sweep angle.

Experimental data have been obtained in the Langley 19-foot pressure tunnel on a wing of aspect ratio 8.02, 45° sweepback of the quarter-chord line, taper ratio of 0.45, and NACA 63_1A012 airfoil sections parallel to the plane of symmetry. Pressure data were available from 8 spanwise stations, including one at the plane of symmetry. The present report compares the loadings computed by the second-order lifting-line method of Weissinger (ref. 2) and the lifting-surface methods of Falkner (ref. 3) and Multhopp (ref. 4) with the experimental loading.

The effects of the number and distribution of spanwise control points, the chordwise distribution of control points, the root-section discontinuity, and the chordwise distribution of circulation on the spanwise loading, lift-curve slope, center of pressure, pitching moment, and induced drag are examined and discussed. The applicability of the calculations at high lift coefficients is also investigated. Also presented are spanwise loadings predicted by the rapid approximate methods of Diederich (ref. 5) and Jones (ref. 6).

SYMBOLS

$\frac{c_l c}{\bar{c}}$	wing loading parameter
$\frac{c_l c}{C_L \bar{c}}$	unit wing loading parameter
c_l	section lift coefficient, $\cos\alpha\int_{LE}^{TE}(S_u-S_l)\,d\left(\frac{x}{c}\right)-\sin\alpha\int_{-\left(\frac{z}{c}\right)_{max}}^{\left(\frac{z}{c}\right)_{max}}(S_r-S_f)\,d\left(\frac{z}{c}\right)$
C_L	wing lift coefficient, $\frac{1}{2}\int_{-1}^{1}\frac{c_l c}{\bar{c}}\,d\eta$ or $\frac{L}{qS_w}$
C_m	wing pitching-moment coefficient
C_D	wing drag coefficient, $\frac{D}{qS_w}$
C_{D_i}	induced-drag coefficient, $\frac{1}{2}\int_{-1}^{1}\frac{c_l c}{\bar{c}}\,\alpha_i\,d\eta$
c	local wing chord, ft
$\bar{c}$	mean wing chord, $\frac{S_w}{b}$, ft
b	wing span, ft
S_w	wing area, sq ft
S	pressure coefficient, $\frac{H-p}{q}$
H	free-stream total pressure, lb/sq ft
p	local static pressure, lb/sq ft
L	lift, lb
D	drag, lb

†Supersedes recently declassified NACA RM L51G30, 1952.

q free-stream dynamic pressure, $\frac{1}{2}\rho V^2$, lb/sq ft

V free-stream velocity, fps.

ρ density of air, slugs/cu ft

x chordwise coordinate, positive rearward, ft

y spanwise coordinate, positive right, ft

z normal coordinate, positive up, ft

η nondimensional spanwise coordinate, $\frac{y}{b/2}$

$\bar{x}$ longitudinal coordinate of center of pressure, ft

$\bar{y}$ lateral coordinate of center of pressure along mean aerodynamic chord, ft

C_{L_α} lift-curve slope per degree

θ angular chordwise coordinate, $\cos^{-1}\left(1-\frac{x}{c/2}\right)$, radians

$\frac{\Delta v_a}{V}$ ratio of increment of local velocity caused by additional type of load distribution to free-stream velocity

$a_0, a_1, \ldots a_{12}$ coefficients of terms in Fourier representation of chordwise loading

α geometric angle of attack, deg

α_i induced angle of attack, deg

Subscripts:

u upper surface

l lower surface

f forward of point of maximum thickness

r rearward of point of maximum thickness

MODEL AND TESTS

The wing tested (ref. 7) had an aspect ratio of 8.02, 45° sweepback of the quarter-chord line, taper ratio of 0.45, NACA 63_1A012 airfoil sections, and no geometric twist (fig. 1). The wing was constructed with a solid steel core, and measurements of the twist due to aerodynamic loading showed it to vary linearly with lift coefficient. Under the test conditions of the subject wing, the twist amounted to about 0.2° at $C_L=1.0$.

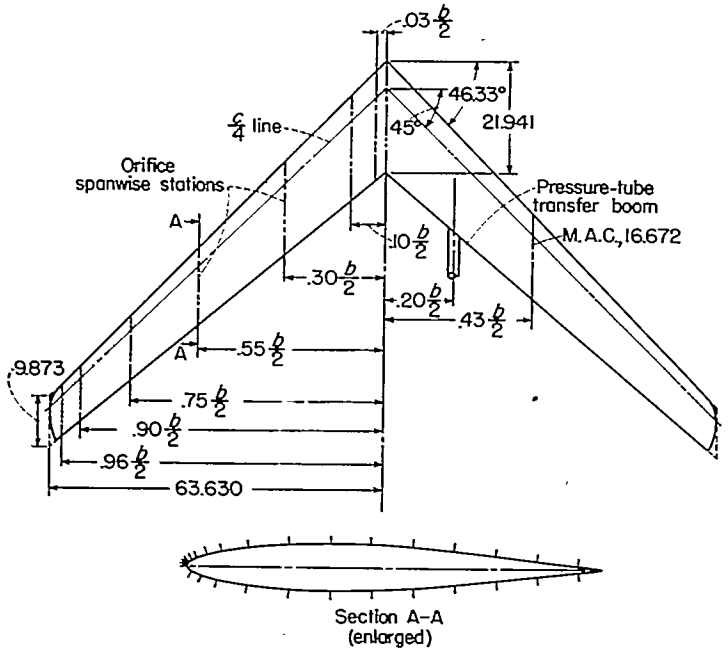

FIGURE 1.—Geometric characteristics of model. Aspect ratio, 8.02; taper ratio, 0.45; airfoil section, NACA 63_1A012. (Dimensions are in inches except as noted.)

Pressure readings were obtained at 225 pressure orifices distributed among 8 stations located at the plane of symmetry and at 3, 10, 30, 55, 75, 90, and 96 percent of the semispan. A typical chordwise distribution of the orifices is shown in figure 1. Further details of the orifice locations and the model can be found in reference 7.

The tests were conducted in the Langley 19-foot pressure tunnel at a Reynolds number of 4.0×10^6, based on the wing mean aerodynamic chord, which, for the tunnel pressure (33 lb/sq in. abs) used in these tests, corresponded to a Mach number of 0.19. Pressure distributions were obtained through the angle-of-attack range from −1° to 30°.

The wing was also tested with two full-chord fences located at $0.575b/2$ and $0.800b/2$ and one partial-chord fence extending over the rearmost 65 percent of the chord at $0.890b/2$. Similar pressure measurements were made with this configuration except that no pressure data were obtained at 3 percent of the semispan.

REDUCTION AND CORRECTION OF DATA

The pressure coefficients were numerically integrated at each station to obtain section data (lift, drag, and pitching moment). The span loadings indicated that a lift distribution existed at zero lift which, flow measurements showed, was due mainly to a spanwise stream-angle variation in the region occupied by the model. Inasmuch as no satisfactory method for correcting the individual pressure coefficients exists, the experimental basic loading was subtracted from the integrated section data. Further details can be found in reference 7.

The measured twist of the wing due to deflection under load indicated that the root sections were at about 0.2° greater angle of attack at a lift coefficient of 1.0 than were the tip sections. The jet-boundary-induced angle variation, calculated by the method of reference 8, showed that at the same lift coefficient the tip sections were effectively at about 0.2° greater angle of attack than the root section. Thus, the sum of the jet-boundary-induced angle and the twist of the wing due to load resulted in a nearly constant spanwise angle-of-attack distribution, so that no correction to the spanwise lift distribution was required to correct for either angle variation.

Jet-boundary corrections and twist-due-to-load corrections were applied to the total wing forces and moments by using the weighted average of the remaining spanwise angle distribution. These corrections which are applied to the angle of attack, drag, and pitching moments are listed below. The following jet-boundary corrections, as calculated by the method of reference 8, are also listed (although not used in this report) for the convenience of the reader:

	Jet-boundary corrections (ref. 8)	Jet-boundary and twist-due-to-load corrections
$\Delta\alpha$, deg	$0.387C_L$	$0.470C_L$
ΔC_D	$0.00634C_L^2$	$0.00776C_L^2$
ΔC_m	$0.0035C_L$	$0.00325C_L$

Tare and interference corrections have also been applied to the force-test data, and force-test pitching-moment coefficients have also been corrected for the pitching moment due to the zero-lift wing loading. Spanwise integration of the section force and moment distributions obtained from the pressure tests resulted in total wing lift, drag, and pitching-moment coefficients.

An indication of the accuracy of the data can be seen in figure 2, where the total wing lift, drag, and pitching-moment coefficients, as determined from both force-test measurements and pressure-distribution measurements, are plotted. The force-test zero-lift drag coefficient has been added to the drag coefficients determined by pressure measurements in an attempt to take into account partially the friction forces. The agreement of the coefficients determined by the two methods of testing is very good.

COMPARISON OF EXPERIMENTAL LOADING WITH CALCULATED LOADINGS

In the present section, the experimental loading is compared with loadings calculated by the standard methods proposed by Weissinger, Falkner, and Multhopp, as well as by modifications of these methods. These methods are summarized in table I.

SYSTEM OF IDENTIFYING SOLUTIONS

All the methods of calculation recognize the fact that the flow through the wing must be zero, and this condition is fulfilled mathematically at a discrete number of points (called control points). The number and distribution of these points then form a convenient means of identifying solutions. The identification system used in this report employs two numbers. The first number following the name refers to the number of spanwise stations at which control points are located, while the second number is the number of chordwise control points at each station. For example, Falkner 6 × 3 refers to a Falkner solution utilizing 3 chordwise control points at each of 6 spanwise stations.

SPANWISE LOAD DISTRIBUTION

As a basis for comparison, the experimental loading at an angle of attack of 4.7° was chosen. Section lift-curve data indicate that at this angle the force characteristics are still linear and tip separation has not occurred. Practically identical loadings were found at lower angles of attack. For most of the comparisons, data are presented for unit lift coefficient to facilitate the comparisons of the shapes of the spanwise load distributions.

Three calculated loadings are compared with the experimental loading in figure 3. These loadings were calculated by using the procedures recommended by the authors. In the Weissinger 7 × 1 solution the circulation is assumed to be concentrated along the quarter-chord line and to vary continuously across the span. The downwash is then calculated at 7 spanwise control points on the three-quarter-chord line. No attempt is made to take into account the discontinuity in plan form at the root station. The loading calculated by this method is too high over the outboard portions. In the

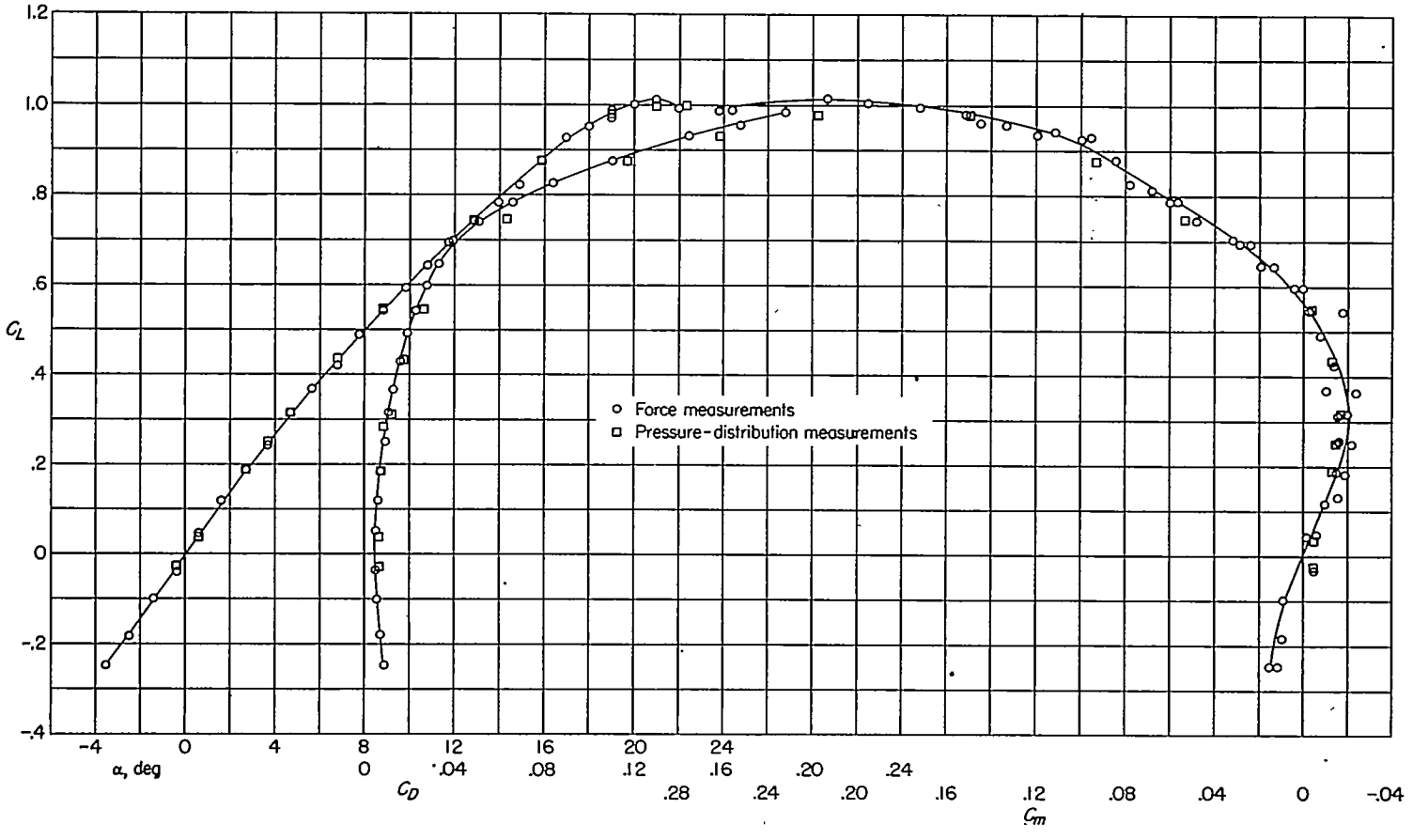

FIGURE 2.—Variation of lift coefficient with angle of attack, drag coefficient, and pitching-moment coefficient obtained by total-force measurements and pressure measurements.

TABLE I. COMPARISON OF METHODS OF CALCULATING LOAD DISTRIBUTION

Method	Spanwise location of control points	Chordwise location of control points	Special treatment of root section	Chordwise distribution of vorticity
Weissinger:				
7×1 standard	0, 0.3827, 0.7071, 0.9239	$\frac{3c}{4}$	None	Concentrated at $\frac{c}{4}$
15×1	0, 0.1951, 0.3827, 0.5556, 0.7071, 0.8315, 0.9239, 0.9808	$\frac{3c}{4}$	None	Concentrated at $\frac{c}{4}$
Falkner:				
6×3 standard	0.2, 0.5, 0.8	$\frac{15c}{24}$, $\frac{19c}{24}$, $\frac{23c}{24}$	None	Concentrated at $\frac{c}{24}$, $\frac{5c}{24}$, $\frac{9c}{24}$, $\frac{13c}{24}$, $\frac{17c}{24}$, $\frac{21c}{24}$
5×3	0, 0.5, 0.8	$\frac{15c}{25}$, $\frac{19c}{24}$, $\frac{23c}{24}$	None	Concentrated at $\frac{c}{24}$, $\frac{5c}{24}$, $\frac{9c}{24}$, $\frac{13c}{24}$, $\frac{17c}{24}$, $\frac{21c}{24}$
19×1 (modified)	0, 0.1, 0.2, 0.3, 0.4, 0.5, 0.6, 0.7, 0.8, 0.9	$\frac{3c}{4}$	None	Concentrated at $\frac{c}{4}$
Multhopp:				
7×1	0, 0.3827, 0.7071, 0.9239	$\frac{3c}{4}$	Bent root station	Distributed over chord $\left(a_0 \cot \frac{\theta}{2}\right)$
15×1	0, 0.1951, 0.3827, 0.5556, 0.7071, 0.8315, 0.9239, 0.9808	$\frac{3c}{4}$	Bent root station	Distributed over chord $\left(a_0 \cot \frac{\theta}{2}\right)$
15×1 (modified)	0, 0.1951, 0.3827, 0.5556, 0.7071, 0.8315, 0.9239, 0.9808	$\frac{3c}{4}$	None	Distributed over chord $\left(a_0 \cot \frac{\theta}{2}\right)$
23×1 standard	0, 0.1305, 0.2588, 0.3827, 0.500, 0.6088, 0.7071, 0.7934, 0.8660, 0.9239, 0.9659, 0.9914	$\frac{3c}{4}$	Bent root station	Distributed over chord $\left(a_0 \cot \frac{\theta}{2}\right)$
15×2	0, 0.1951, 0.3287, 0.5556, 0.7071, 0.8315, 0.9239, 0.9808	0.3455c and 0.9045c	Bent root station	Distributed over chord $\left(a_0 \cot \frac{\theta}{2} + a_1 \sin \theta\right)$

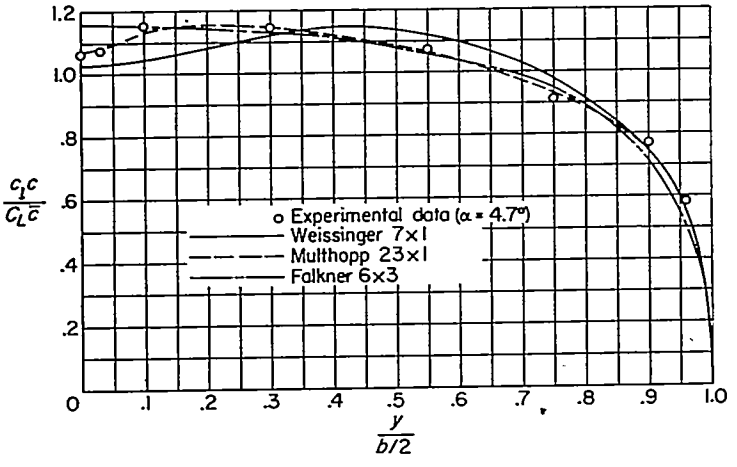

FIGURE 3.—Experimental span load distribution compared with span load distributions calculated by several standard procedures.

Falkner 6 × 3 solution a particular form of a spanwise and a chordwise distribution of circulation is assumed in order to define the strength of a number (21) of discrete horseshoe vortices distributed over the span at each of 6 chordwise locations. The downwash condition is fulfilled at 3 chordwise control points at each of 6 spanwise stations. No attempt is made to take into account the root-station discontinuity. The agreement is fair except at the root stations, where the experimental dip in loading is not predicted. The Multhopp 23 × 1 solution assumes a continuous spanwise and chordwise variation of circulation. The downwash condition is fulfilled at 23 spanwise control points (approximately 3 × aspect ratio). The discontinuity is treated by modifying the geometric characteristics of the wing at the root. Good agreement with experiment is obtained with this method.

All the calculated loadings differ from one another. The differences are, of course, attributed to the differences in the assumed loading and the control points used to arrive at a solution. To check the influence of the number and location of the spanwise and chordwise control points and the root-section discontinuity, some of the authors' recommendations were disregarded and variations of the methods were used to calculate the loadings.

Number and location of spanwise control points.—Weissinger states in reference 2 that, for straight wings of moderate aspect ratio, 7 control points are all that are necessary for an accurate prediction of the load distribution. Schlichting and Kahlert (ref. 9), however, have indicated that, for swept wings, if the aspect ratio is increased to infinity, the use of any finite number of control points will result in a triangularly shaped loading with the minimum at the root. Multhopp states in reference 4 that for accuracy the number of control points should be about three times the aspect ratio. To examine more closely the effect of the number of spanwise control points, several solutions have been carried out in which this parameter was varied. The Weissinger method was carried out by using 15 control points and the Multhopp method was carried out by using 7 and 15 control points. For each solution, it was necessary to calculate the constants embodied in the simultaneous equations. The number of equations to be solved was equal to the number of control points in a semispan.

Figure 4 (a) compares the Weissinger 7 × 1 and 15 × 1 solutions. The 7-point solution predicts too high a loading

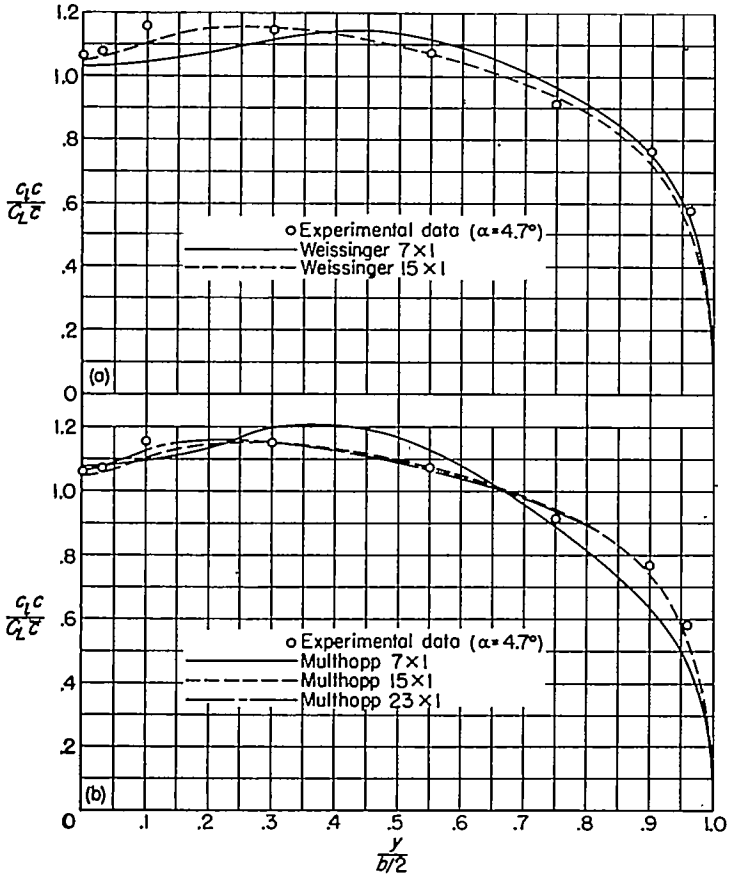

(a) Weissinger methods.
(b) Multhopp methods.

FIGURE 4.—Effect of number of spanwise control points on the span load distribution.

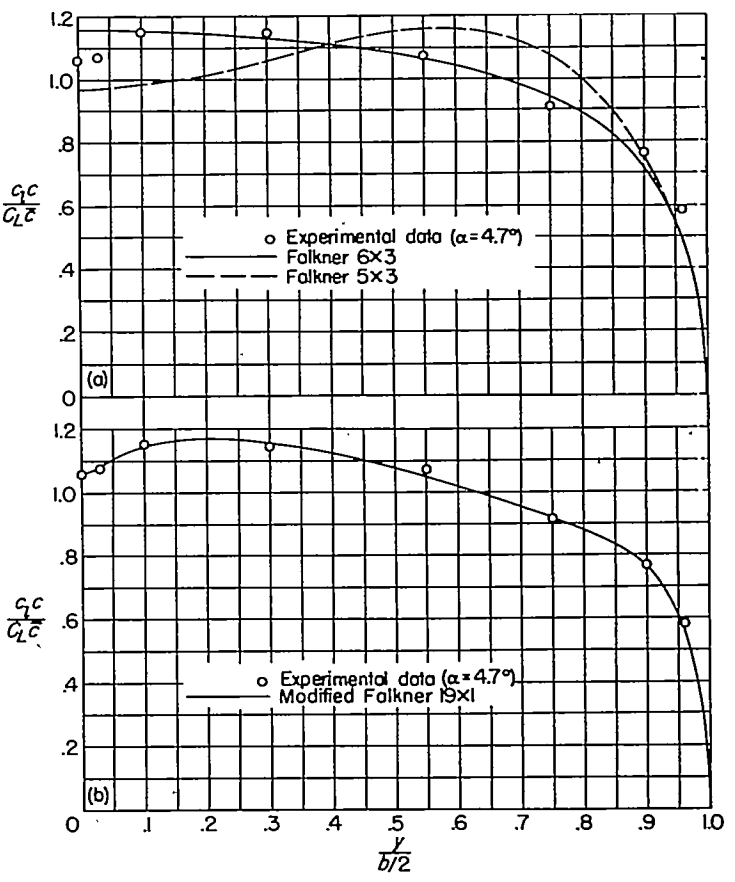

(a) Falkner methods.
(b) Modified Falkner method.

FIGURE 5.—Effect of location and number of spanwise control points on the span load distribution.

toward the tip and too low and broad a loading near the root. This type of loading results because the control points (at $\eta = 0$, 0.3827, 0.7071, and 0.9239) miss the essential variations in the loading, as can be seen from the experimental data. In addition, the lower order approximation for the assumed spanwise loading does not involve enough terms to describe accurately the load distribution. Increasing the number of control points to 15 produces a more accurate loading, since now the spacing of the control points is closer and more terms are used in the assumed loading.

Figure 4 (b) compares the experimental data with Multhopp's 7 × 1, 15 × 1, and 23 × 1 solutions. The same logic applies here—namely, the accuracy of the predicted load shape increases as the number of spanwise control points increases.

Obviously, as the number of control points is increased, the time required to arrive at a solution is also increased. From figure 4, it appears as if the use of 15 control points for either the Weissinger or Multhopp method will result in relatively accurate loadings with a minimum of time required for the solution.

In order to predict accurately the loading in the neighborhood of the root, it was necessary to locate control points in this region. Since Falkner suggests the opposite view in reference 10, another Falkner solution was carried out, in which only the location of the control points was varied. Figure 5 (a) compares the experimental loading with the calculated loadings obtained with the Falkner 6 × 3 solution (control points at $\eta = 0.2$, 0.5, and 0.8) and the Falkner 5 × 3 solution (control points at $\eta = 0$, 0.5, and 0.8). Without the control point at the center section, the center minimum is not predicted. With the control point at the center section, however, the drop in loading is carried over too far outboard. As previously explained, the effect results from too few control points.

The methods used on unswept wings are such that a majority of the control points are located at the tip sections where the loading varies rapidly. Since a drop in loading is also experienced over the central sections of swept wings, it was felt that most of the increase in accuracy when the number of control points was increased was due to the close spacing of the control points at the root stations. A preliminary study was made to investigate this point more fully by using control points at the plane of symmetry and at 0.1b/2 intervals outboard along the span. The method of reference 11, which was set up to calculate the downwash resulting from a given loading, was inverted so that the loading required to induce a given downwash could be calculated. This method employs a simplified vortex representation similar to that used by Falkner but does not use the same mathematical techniques and will be referred to as the modified Falkner 19×1 method. Twenty-one horseshoe vortices were distributed over the span along the quarter-chord line, as in reference 11, and the downwash was calcu-

lated at 19 control points on the three-quarter-chord line. Since the loading is symmetrical, only 10 independent equations, each with 11 unknown loadings, are obtained. The strength of the tip vortex was assumed to be given in terms of the two adjacent vortices by a series of the type $Ax^{1/2}+Bx^{3/2}$, where x is the distance inboard of the tip. The resulting equation

$$\left(\frac{c_l c}{C_L \bar{c}}\right)_{\eta=0.9625}=0.995\left(\frac{c_l c}{C_L \bar{c}}\right)_{\eta=0.9}-0.271\left(\frac{c_l c}{C_L \bar{c}}\right)_{\eta=0.8}$$

was substituted into the 10 equations to eliminate one unknown. The equations were then solved for the remaining 10 unknown loadings. No attempt was made to take into account the root-section discontinuity. The resulting loading (fig. 5(b)) almost duplicates the experimental loading.

For an accurate prediction of the span loading, it is apparently necessary that the number and location of the control points be such that no essential variation of the loading is missed and that the assumed series for the spanwise loading be of high enough order to fit the loading curve.

Chordwise distribution of control points.—Figure 6 provides a comparison of the experimental loading with that calculated by the Multhopp 15×1 and 15×2 solutions. It can be seen that the two loadings are in agreement except at the root stations. In the Multhopp method of calculation the wing sections are replaced by the mean lines and the chordwise distribution of circulation is given by a finite number of trigonometric terms. For the 15×1 solution, Multhopp assumes that this distribution is of the form $a_0 \cot \theta/2$ (which is the theoretical distribution of circulation on a flat plate at an angle of attack) and calculates the downwash at the three-quarter-chord line. For two-dimensional flow, this assumed circulation will produce a constant downwash angle along the chord. However, it can be shown for two-dimensional flow that, if the chordwise distribution of circulation is not purely of the cotangent form but is of the form $a_0 \cot \frac{\theta}{2}+a_1 \sin \theta$, where the additional term corresponds to circular-arc camber, the downwash angle at the three-quarter-chord point remains unchanged provided that the same total lift is considered. Effectively, then, using this assumed loading ($a_0 \cot \theta/2$) and calculating the downwash at the three-quarter-chord line will allow for some camber effect in the solution. For the 15×2 solution, Multhopp assumes a distribution of the form $a_0 \cot \frac{\theta}{2}+a_1 \sin \theta$ (which is the distribution of circulation along a circular arc at an angle of attack in two-dimensional flow) and calculates the downwash at $0.9045c$ and $0.3455c$. Again, the significance of these two points is that the presence of any proportion of a third term of the series, $a_2 \sin 2\theta$ (due to reflex camber), will not affect the induced downwash at these two points for a given lift coefficient and pitching-moment coefficient.

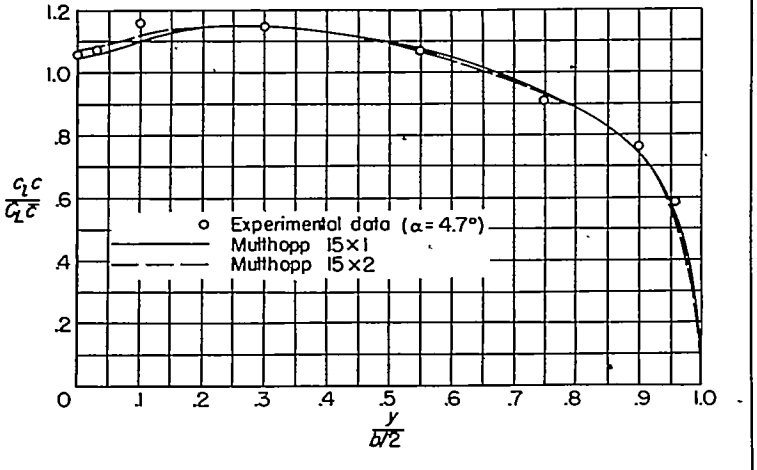

FIGURE 6.—Effect of number of chordwise control points on span load distribution.

The wing investigated was of finite thickness and had a flat mean line, but three-dimensional effects might be expected to induce camber. A Fourier analysis of the experimental chordwise loading obtained on the wing (three-dimensional) showed that the induced camber of the wing is practically constant over the span, except in the vicinity of the root (and to a lesser degree, at the tip), where the induced camber was more pronounced. The analysis showed the terms $a_0 \cot \theta/2$, $a_1 \sin \theta$, and $a_2 \sin 2\theta$ to be significant and of the same order of magnitude. A similar analysis was made for the theoretical two-dimensional loading on the NACA 63_1A012 airfoil sections as given in the $\Delta v_a/V$ tables of reference 12. (The sections normal to the leading edge are actually about 16.3 percent thick, but the tables did not give any values for this thickness ratio.) The relative values of a_0, a_1, a_2, . . . were found to be very nearly the same as for most of the three-dimensional wing. Thus, the relatively large values of a_1 and a_2 arise as a result of thickness and are not due to induced camber (except at the root and tip). Since the induced camber at the root is more significant in the experimental loading, it is not surprising that the 15×1 and 15×2 solutions differ in this region. However, although the 15×2 solution should be more nearly correct, it can be seen from figure 6 that both loadings are within the experimental accuracy of the data.

Root-section discontinuity.—Experimental investigations on swept wings have shown that the pressure isobars at the root sections are continuously curved rather than sharply bent so that there is no discontinuity in flow. This curving of the pressure isobars at the root produces a flatter chordwise distribution of load with a more rearward center of pressure. Both Multhopp (ref. 4) and Schlichting and Kahlert (ref. 9) recommend that corrective measures be applied at the root sections to take into account this phenomenon. Only the Multhopp method was available for comparison. For the standard solution, Multhopp proposes the use of an equivalent wing which has the same geometry as the actual wing with the exception that the root chord is shortened and shifted rearward in a specified manner so as to round off the apex of the wing. A modified Multhopp solution can be found by neglecting this proposal. In figure 7, the experimental loading is compared with two Multhopp 15×1 solutions. The standard solution shows good agreement between theory and experiment. As would be expected, the major effect was at the root stations where the modified solution predicts a lower loading than the standard solution. In general, it appears that the Multhopp correction to take into account the bending of the isobars at the

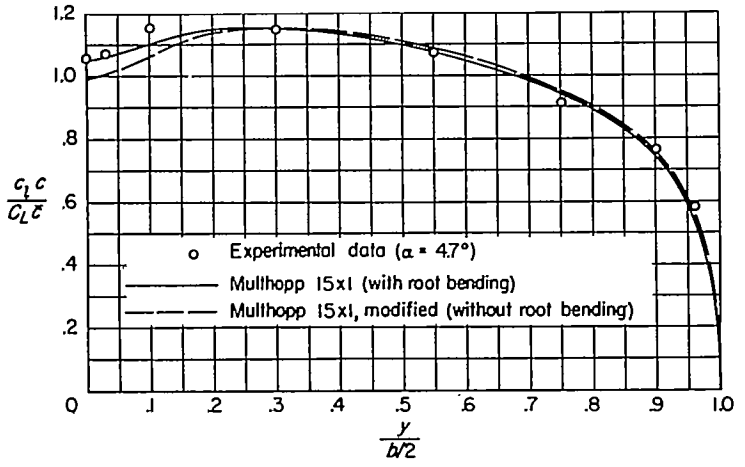

FIGURE 7.—Effect of the Multhopp treatment of bending at the root stations on the span load distribution.

root stations has a small but beneficial effect on the span loading for a wing of this aspect ratio. For wings of smaller aspect ratio, however, the correction may be of greater importance.

Chordwise distribution of circulation.—When the Weissinger 15×1 solution is compared with the modified Multhopp 15×1 solution (fig. 8), the effect of the chordwise distribution of circulation on the span load distribution can be seen. As previously stated, in the Weissinger method the circulation is assumed to be concentrated at the quarter-chord line, whereas in the Multhopp method a chordwise distribution of the form $a_0 \cot \theta/2$ is assumed. In both methods the downwash is computed at the three-quarter-chord line. The effect of the assumed distribution can be seen to be largest at the root stations where the Multhopp lifting-surface theory predicts a lower loading than the Weissinger second-order lifting-line theory. The total effect appears to be of small importance, and very possibly, some of the difference may be due to the differences in the computational techniques rather than to differences in the basic methods.

Rapid approximate methods.—The load distributions obtained by two rapid approximate methods are shown in figure 9. The method indicated by equation (1) of reference 5 predicts a load distribution which is in fair agreement with experiment. About 10 minutes was required for a solution.

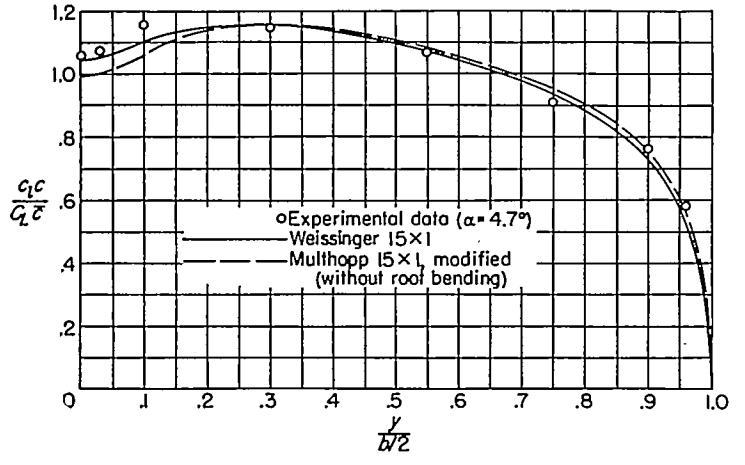

FIGURE 8.—Effect of an assumed chordwise circulation distribution.

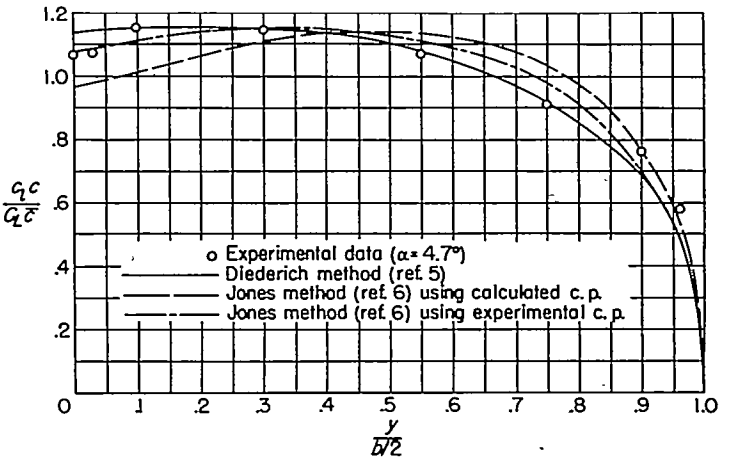

FIGURE 9.—Comparison of span load distributions obtained by rapid approximate methods.

The loading predicted by the method of reference 6, which is based upon the assumption that wings with similar spanwise centers of pressure have similar load distributions, has been presented for two cases. The first loading was obtained by using the center-of-pressure location calculated by the method of reference 6, whereas the second loading was obtained by using the experimental center-of-pressure location. The first loading is in rather poor agreement with experiment. The second loading is in somewhat better agreement with experiment. Since the method of reference 6 is based upon results obtained by the Weissinger 7×1 solution which has been shown to be inadequate for this wing, it is not surprising that corresponding inaccuracies exist. This method is extremely rapid, however, and required less than 5 minutes for each loading.

High lift coefficients.—All the methods of calculation assume that viscous effects are negligible, that is, that boundary layers are very thin and, in particular, that the flow is unseparated. It is of interest to compare the calculated loadings with the measured loadings at high lift coefficients. Figure 10 presents experimental loadings obtained on the

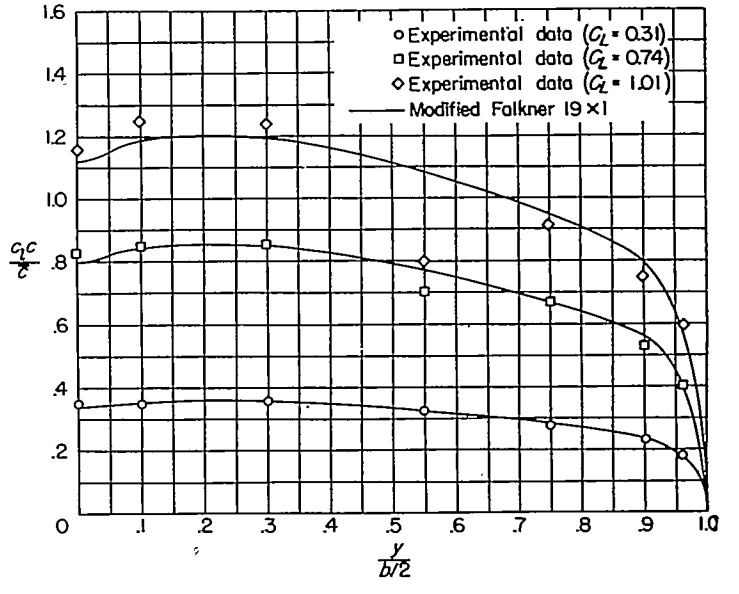

FIGURE 10.—Calculated and experimental span load distribution at several values of lift coefficients for the wing equipped with fences.

wing with fences at three lift coefficients. This configuration was used rather than the plain wing because separation occurred at low values of the lift coefficient on the plain wing, and, obviously, once the flow separates, the solutions are invalid. The calculated curve presented is the modified Falkner 19×1 solution since it predicts the best loading shape at low lift coefficients. At the moderate lift coefficient (0.74), the agreement between the calculated curve and experimental values is still good. At the highest lift coefficient (1.01), the agreement is reasonable, although tip stall has begun. It should be noted that the large irregularity at $0.55b/2$ is due to the fact that this station is just inboard of a fence and is apparently in a localized region of separation at both the moderate and high lift coefficients.

LIFT-CURVE SLOPE

The experimental lift-curve slope determined from both force and pressure measurements is 0.069 per degree through zero lift. This slope is maintained up to an angle of attack of about 5°, beyond which the slope gradually decreases, as shown in figure 11.

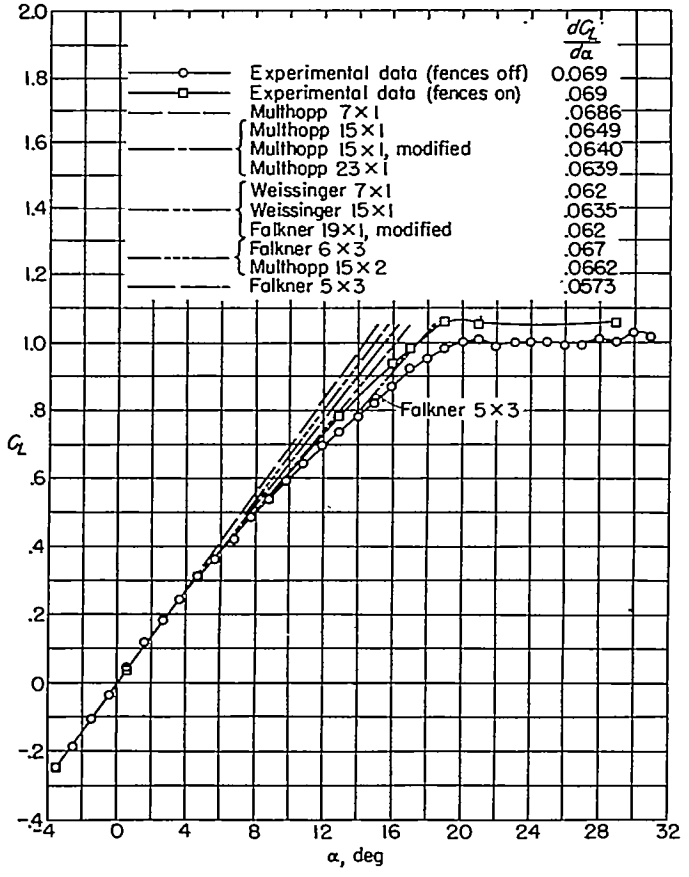

FIGURE 11.—Comparison of experimental lift-curve slope with calculated values.

The lift-curve slopes predicted by the various method of calculation are also indicated in figure 11. The number of spanwise control points utilized had a marked effect on the slope predicted by any one method. For the Weissinger and Falkner solutions, as the number of spanwise control points is increased, the value of the lift-curve slope is increased. The opposite, however, is true of the Multhopp method, where an increasing number of control points causes a decrease in lift-curve slope. It appears as if both the Weissinger and Multhopp solutions may be converging toward a common value of lift-curve slope as the number of control points is increased, although there are not enough solutions to examine this point further.

Schlichting and Kahlert (ref. 9), in an analysis of the Mutterperl (ref. 13) and Weissinger (ref. 2) methods, conclude that by not locating a control point at the center section a higher lift-curve slope will result. A comparison of the Falkner 6×3 and 5×3 solutions appears to verify this conclusion. Each solution uses 3 chordwise control points in a semispan and an equal number of terms in the approximation for the assumed span loading. A marked decrease in the lift-curve slope results partially from locating a control point at the plane of symmetry and partially from decreasing the number of spanwise control points. It would seem, then, that the close agreement between the Falkner 6×3 solution and experiment, with regard to the lift-curve slope, depends to a large extent upon the particular choice of control-point location.

Reference 9 also points out that, in order for the lift-curve slope to reach the correct value when a control point is located at the center section, special treatment must be given to the center section to take into account the discontinuity in plan form. When the Multhopp 15×1 solution, where the center section is rounded, is compared with the Multhopp 15×1 modified solution, the increase is evident. The addition of a corrective term at the plane of symmetry increases the lift-curve slope. In this instance the increase was only 1.3 percent of the experimental value, which is of the same order of magnitude as reported in reference 9.

All the methods of calculation (which are based on thin-airfoil theory) underestimate the lift-curve slope, and those methods which result in a fairly accurate load shape underestimate the slope by about 8 percent. This difference is presumably due to the finite thickness of the airfoil and is, in fact, equal to the difference found experimentally between the two-dimensional lift-curve slope for NACA 63-series airfoil sections of about this thickness ratio (about 16.2 percent normal to the leading edge) and the slope given by two-dimensional thin-airfoil theory (see ref. 14). The theoretical value of the lift-curve slope for these thick sections exceeds that for thin airfoils by about 12 percent.

CENTER OF PRESSURE

The spanwise position of the center of pressure (fig. 12) is predicted with the greatest accuracy by the methods that most accurately predict the spanwise load distribution. Obviously, then, what has previously been said about an accurate prediction of load shape applies here—the number and location of the control points has the largest influence on the prediction of the spanwise center of pressure.

The chordwise position of the center of pressure is also shown in figure 12. Except for the Falkner 5×3 and 6×3 solutions and the Multhopp 15×2 solution, the chordwise location of the center of pressure has been assumed to be on the quarter-chord line for lack of anything better. This assumption is equivalent to assuming that the section acts as a flat plate and that the higher harmonics are zero. For the Falkner 5×3 and 6×3 solutions and Multhopp 15×2 solution, the wing center of pressure is not necessarily at the quarter-chord line of the wing. For this wing, however, the calculations (in which the unknown second harmonic was neglected in the Multhopp solution) showed the chordwise center of pressure to be essentially on the quarter-chord line.

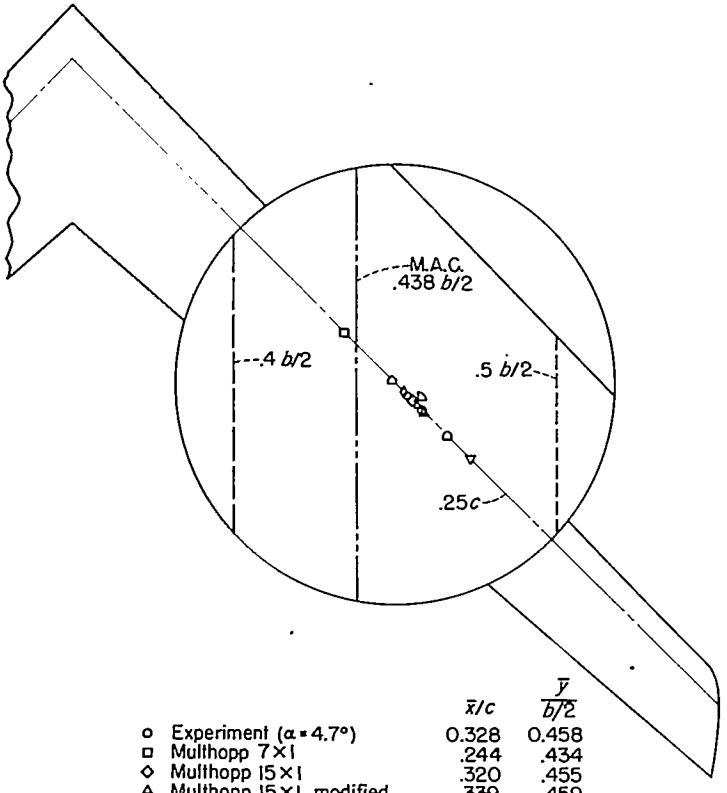

		$\frac{\bar{x}}{c}$	$\frac{\bar{y}}{b/2}$
○	Experiment (α = 4.7°)	0.328	0.458
□	Multhopp 7×1	.244	.434
◇	Multhopp 15×1	.320	.455
△	Multhopp 15×1, modified	.339	.459
▷	Multhopp 23×1	.331	.457
▷	Multhopp 15×2	.311	.458
▫	Weissinger 7×1	.363	.466
○	Weissinger 15×1	.316	.454
◇	Falkner 19×1, modified	.313	.453
△	Falkner 6×3	.297	.449
▽	Falkner 5×3	.390	.473

FIGURE 12.—Location of experimental and calculated center of pressure.

The spanwise variations of the local center of pressure predicted by the Falkner 6×3 and 5×3 solutions and the Multhopp 15×2 solution are shown in figure 13. For comparison, the experimental data for four angles of attack for both the plain wing and the wing with fences are shown as unconnected symbols. The lower angle of attack (2.7°) is representative of the low angle range. It can be seen that, as the angle of attack is increased for the plain wing, tip stall causes the local centers of pressure to move rearward. With fences, this movement is somewhat retarded until the wing stalls (α=21.0°). It is interesting to note that at α=17.0° (C_L=1.01), the shape of the spanwise loading curve for the wing with the fences is still very similar to the curves for the lower angles of attack as shown in figure 10, despite the fact that a considerable rearward movement of the local centers of pressure is shown in figure 13. The values calculated by the Multhopp 15×2 method are in good agreement with experiment and predict the rearward locations at the root and the forward locations at the tip. The standard Falkner 6×3 solution is only in fair agreement with experiment, and it can be seen that, without special handling at the root section (such as given in ref. 9), the rearward shift of the centers of pressure is not predicted. The Falkner 5×3 solution predicts the center of pressure too far rearward over the inboard portions of the wing and too far forward over the outboard portions of the span.

WING PITCHING MOMENT

It is of interest to apply the previously mentioned parameters to the prediction of the overall wing characteristics. In figure 14 is plotted the experimental pitching-moment coefficient against lift coefficient for the plain wing and the wing with fences, as well as various calculated curves. The pitching moment due to lift is a function of the center-of-pressure location; thus good agreement is obtained for the more accurate loading methods. It is interesting to note that the spread of the curves represents a center-of-pressure variation of about 12 percent mean aerodynamic chord.

INDUCED DRAG

The calculated variation of induced-drag coefficient with lift coefficient is shown in figure 15. Most of the calculated curves fall in a narrow band with about a 5-percent spread. These calculations are dependent upon both the lift-curve slope and the load distribution, and it appears as if any reasonable estimate of these characteristics will predict the induced drag fairly well. The load shape resulting from the Falkner 5×3 solution combined with the low lift-curve slope, however, predicts an induced-drag coefficient about 30 percent higher than those predicted by the other solutions.

308555—50——76

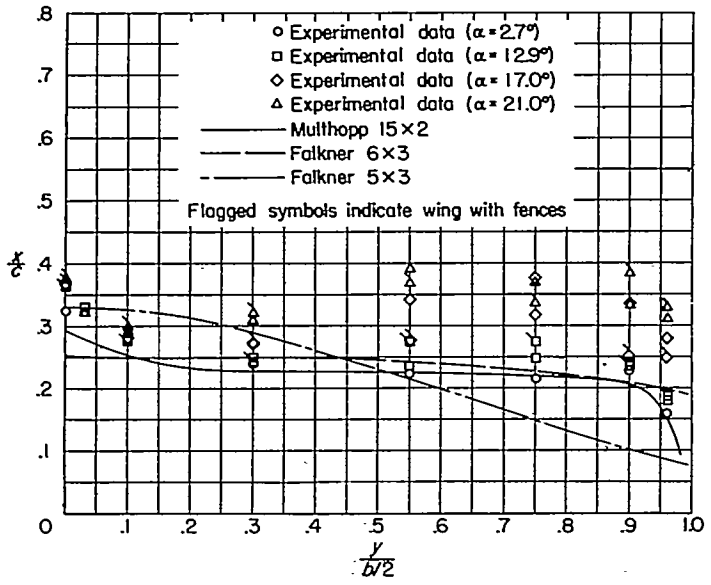

FIGURE 13.—Calculated and experimental chordwise location of the local center of pressure across the span.

CONCLUDING REMARKS

Experimental force and moment data obtained by pressure measurements on a wing of aspect ratio 8.02, 45° sweepback of the quarter-chord line, taper ratio of 0.45, and NACA 63_1A012 airfoil sections have been compared with the calculated loadings obtained by the standard methods of Weissinger, Falkner, and Multhopp.

With regard to the shape of the spanwise loading distribution, the most accurate load shape was predicted by the Multhopp 23×1 solution. The standard Falkner 6×3 solution did not predict the experimental drop in loading at the root stations.

All the methods predicted similar load shapes provided that a sufficient number of spanwise control points were used in the solution. At least 15 were necessary for this wing.

It was found that a slight improvement in lift-curve slope and loading shape resulted when the Multhopp scheme of rounding the apex of the wing was used.

The Multhopp method with either one or two chordwise control points predicted essentially the same spanwise loading, except at the root stations.

Those methods which predicted the loading shape fairly accurately predicted the lift-curve slope about 8 percent too low. The low estimate is probably caused by the finite thickness of the wing.

The spanwise variation of the chordwise position of the center of pressure was fairly accurately predicted by the Multhopp method with 2 chordwise control points.

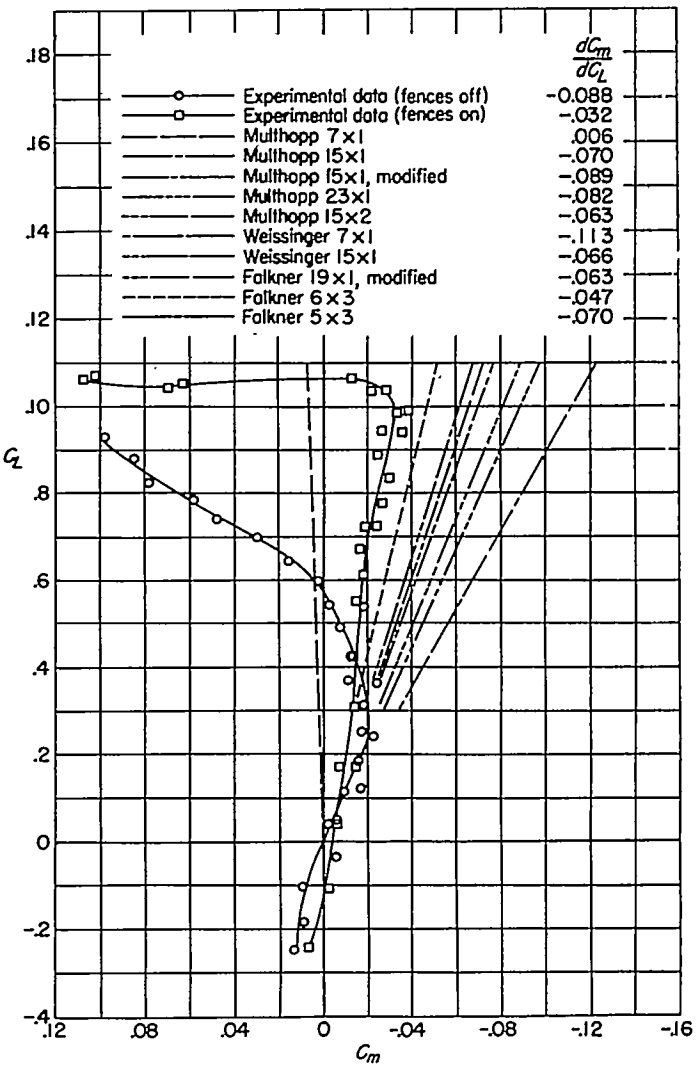

FIGURE 14.—Calculated and experimental variation of pitching-moment coefficient with lift coefficient.

It appears as if the Multhopp or the Weissinger method will result in the best overall compromise between lift-curve slope and load shape, provided enough control points are used in the solution. For an extremely rapid estimate of the load shape, Diederich's method predicted a reasonably accurate loading for this wing.

LANGLEY AERONAUTICAL LABORATORY,
NATIONAL ADVISORY COMMITTEE FOR AERONAUTICS,
LANGLEY FIELD, VA., *August 14, 1951.*

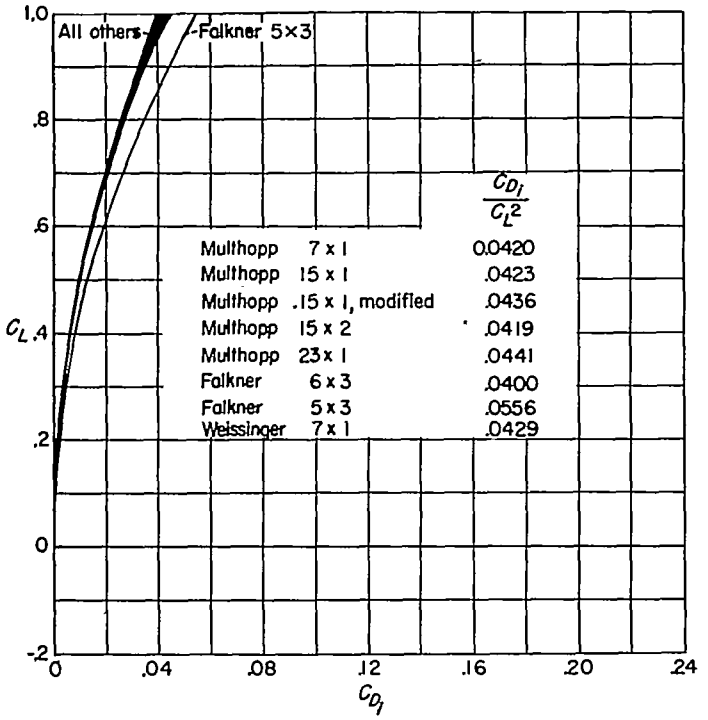

FIGURE 15.—Calculated variation of induced-drag coefficient with lift coefficient.

REFERENCES

1. Van Dorn, Nicholas H., and DeYoung, John: A Comparison of Three Theoretical Methods of Calculating Span Load Distribution on Swept Wings. NACA TN 1476, 1947. (Supersedes NACA RM A7C31.)
2. Weissinger, J.: The Lift Distribution of Swept-Back Wings. NACA TM 1120, 1947.
3. Falkner, V. M.: The Calculation of Aerodynamic Loading on Surfaces of Any Shape. R. & M. No. 1910, British A. R. C., 1943.
4. Multhopp, H.: Methods for Calculating the Lift Distribution of Wings (Subsonic Lifting Surface Theory). Rep. No. Aero. 2353, British R. A. E., Jan. 1950.
5. Diederich, Franklin W.: Approximate Aerodynamic Influence Coefficients for Wings of Arbitrary Plan Form in Subsonic Flow. NACA TN 2092, 1950.
6. Jones, R. Stanton: An Empirical Method for Rapidly Determining the Loading Distributions on Swept Back Wings. Rep. No. 32, College of Aero., Cranfield (British), Jan. 1950.
7. Graham, Robert R.: Low-Speed Characteristics of a 45° Sweptback Wing of Aspect Ratio 8 From Pressure Distributions and Force Tests at Reynolds Numbers From 1,500,000 to 4,800,000. NACA RM L51H13, 1951.
8. Sivells, James C., and Salmi, Rachel M.: Jet-Boundary Corrections for Complete and Semispan Swept Wings in Closed Circular Wind Tunnels. NACA TN 2454, 1951.
9. Schlichting, H., and Kahlert, W.: On the Calculation of the Lift Distribution of Swept Wings. Rep. No. Aero. 2297, British R. A. E., Oct. 1948.
10. Falkner, V. M.: The Solution of Lifting-Plane Problems by Vortex-Lattice Theory. R. & M. No. 2591, British A. R. C., 1947.
11. Diederich, Franklin W.: Charts and Tables for Use in Calculations of Downwash of Wings of Arbitrary Plan Form. NACA TN 2353, 1951.
12. Loftin, Laurence K., Jr.: Theoretical and Experimental Data for a Number of NACA 6A-Series Airfoil Sections. NACA Rep. 903, 1948. (Supersedes NACA TN 1368.)
13. Mutterperl, William: The Calculation of Span Load Distributions on Swept-Back Wings. NACA TN 834, 1941.
14. Abbott, Ira H., Von Doenhoff, Albert E., and Stivers, Louis S., Jr.: Summary of Airfoil Data. NACA Rep. 824, 1945. (Supersedes NACA WR L-560.)